Building Detection in Very High Spatial Resolution Multispectral Images Using the Hit-or-Miss Transform

Katia Stankov and Dong-Chen He

***Abstract*—A method for building detection in very high spatial resolution multispectral images is presented. Buildings are detected using spectral and contextual information. First, potential building locations are enhanced on the basis of the spectral similarity between their roofs. To do this, the eigenvalue-based spectral similarity ratio is proposed. Next, the hit-or-miss transform (HMT) from mathematical morphology is used to assign pixels to buildings. To compute the HMT, fuzzy erosion and dilation are used. Additional processing based on size criteria is needed in some cases to separate buildings from roads. The method is tested on GeoEye and pan-sharpened Ikonos images. The preliminary results are promising.**

***Index Terms*—Building detection, hit-or-miss transform (HMT), mathematical morphology (MM) for multispectral images.**

I. Introduction

THE detection of buildings in very high spatial resolution (VHSR) images is of primary interest as buildings constitute important geospatial data layers in an increasing number of applications [1]. Although individual buildings can be observed in VHSR images, many factors contribute to significant within-feature variation [2]. Sophisticated methods that integrate spatial and spectral information are needed to detect and extract buildings from VHSR images.

Among these methods, mathematical morphology (MM) has already been proven effective for the analysis of spatial structures in remotely sensed images. Information concerning the size of image features provided by the differential morphological profile has been found valuable for the classification of buildings [3] and for the extraction of buildings [4]. The binary morphological template match transform, called hit-or-miss transform (HMT), has been found successful for the detection of buildings [5]. These methods were applied to panchromatic bands; however, the additional spectral information available in some VHSR images may increase the recognition accuracy for buildings [4], [5].

The extension of the binary HMT to grayscale images leads to an operator used to detect locations that are brighter than their neighborhood [6]. In this study, we used this property of the grayscale HMT in order to detect buildings in multispectral images.

The extension of the morphological operators to multispectral images is not straightforward. In order to compare multidimensional pixels, a strategy for ordering their values is required. Although different approaches exist, they do not provide a fully suitable solution for template matching using spectral properties [7]. In the absence of a suitable ordering scheme, we developed a different strategy: In order to apply the grayscale HMT to multispectral images, we transformed them to grayscale images in which potential building locations were enhanced.

The proposed supervised method included the following steps. Several classes were defined according to the roof colors of buildings in the image. For each class, a grayscale image was generated based on the spectral similarity (color) between roofs to improve the low local contrast of VHSR images, which can cause buildings to be undetected [8]. In these images, potential building locations appeared with bright tones. Next, the grayscale HMT was applied to the images generated in the previous step in order to assign pixels to buildings. Additional processing based on size criteria was applied to separate buildings from roads.

This letter is organized as follows. Section II describes the enhancement of buildings on the basis of the spectral similarity between roofs. Section III describes the detection of buildings. Section IV presents the results and discussion. Conclusions are given in Section V.

II. Assessing the Spectral Similarity Between Roofs

The appearance of roofs in VHSR images can be very complex due to the different illumination conditions, the viewing angle, etc. To reduce these effects, in addition to color, we examined the covariance of all bands in the neighborhood of a pixel. For each class of building, we chose a set r_i of reference windows. The reference windows were defined using the most homogeneous parts to guarantee low initial variance. We choose roofs that had very similar color. Each class was processed separately.

To assess the spectral similarity of the neighborhood of each pixel to the spectra of the reference windows, the image was processed with a sliding window $g(p)$, centered on pixel $p(x, y)$ with the coordinates x and y in the image domain. The pixels under the sliding window were added to the pixels of each of the reference windows to create a new data set a_i, referred to

Manuscript received April 15, 2011; revised January 27, 2012 and March 16, 2012; accepted March 26, 2012. Date of publication May 21, 2012; date of current version September 7, 2012.

The authors are with Centre d'Applications et de Recherches en Télédétection, Université de Sherbrooke, Sherbrooke, QC J1K 2R1, Canada (e-mail: katia.stankov@usherbrooke.ca; Dong-Chen.He@USherbrooke.ca).

Color versions of one or more of the figures in this paper are available online at http://ieeexplore.ieee.org.

Digital Object Identifier 10.1109/LGRS.2012.2193552

1545-598X/$31.00 © 2012 IEEE

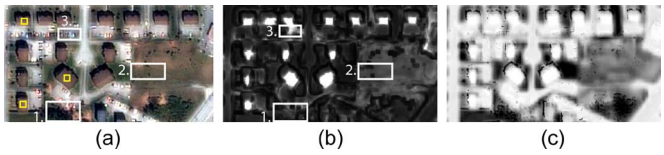

Fig. 1. (a) True color composite of the original Ikonos image. The labeled areas refer to the following: 1) forest; 2) sparse vegetation; and 3) parking lots. The reference windows for brown roofs are shown as yellow squares. (b) Results for SSR. (c) Results for SAM. The results for SAM were inversed: Bright areas correspond to greater spectral similarity to the reference windows.

as the augmented window, with $a_i = g(p) \cup r_i$, where $\cup$ is the set union and r_i is the ith reference window. The goal was to examine how the variance of the reference windows changed in result of the addition. The greater the spectral similarity between the data under the sliding window and the data of the reference windows, the less the variance of the augmented window will change with regard to the initial low variance of the reference windows. As the spectral difference increases, the variance of the augmented window will increase. Because the eigenvalues are proportional to the variance of the data [9], we adopted the ratios between the eigenvalues of the covariance matrices of the reference windows and the augmented windows as an indicator of the change in the variance and, consequently, for the spectral similarity to the reference windows. Lower variance will produce lower eigenvalues [9]; thus, the division of the eigenvalues of the reference windows by the eigenvalues of the augmented windows will yield higher values for higher spectral similarity to the reference windows. Greater spectral differences will lead to at least one high eigenvalue (the first or second), and the values of the division described previously will be lower. We examined the ratios between the first two eigenvalues and retained the minimum between the two divisions. We called this measure the spectral similarity ratio (SSR). It was defined as

$$SSR = \min\left[\max_{i=1,2,\ldots,n}\left(\frac{\lambda_1^{r_i}}{\lambda_1^{a_i(p)}}\right), \max_{i=1,2,\ldots,n}\left(\frac{\lambda_2^{r_i}}{\lambda_2^{a_i(p)}}\right)\right] \quad (1)$$

where $\lambda_1^{r_i}$ and $\lambda_2^{r_i}$ are the first and second eigenvalues of the reference window i ($i = 1, 2, \ldots, n$), n is the number of reference windows, and $\lambda_1^{a_i(p)}$ and $\lambda_2^{a_i(p)}$ are the first and second eigenvalues of the augmented window.

For each class, we obtained a grayscale (SSR) image where the candidate buildings were enhanced. An SSR image with enhanced brown roofs is shown in Fig. 1(b); the reference windows are given on the true color composite in Fig. 1(a).

We applied the SSR to a pan-sharpened (using the method in [10]) Ikonos image (1-m spatial resolution) and to a multispectral GeoEye image (2-m spatial resolution). The size of the reference windows was set according to the size of small buildings: 5×5 for Ikonos and 3×3 for GeoEye. Examples of the reference windows are shown in Fig. 4. The size of the sliding windows was equal to the size of the reference windows. We empirically found that the optimal number of reference windows for each class (color) was three, and the spectral similarity between them computed on the first eigenvalues had to be at least 0.65. More reference windows or less spectral similarity between them resulted in poorer discrimination between buildings and "no buildings."

The SSR could discriminate well between buildings and other homogeneous areas such as lawn, forest, and areas with sparse vegetation [Fig. 1(b)], which formed a dark background in the SSR image. Depending on the color of the roof to be enhanced, pixels situated on objects such as parking lots and roads could also have relatively high SSR values [Fig. 1(b)].

We compared the SSR with the spectral angle mapper (SAM). To measure the spectral similarity between two spectra, SAM portrays each spectrum as a vector in an l-dimensional space [11]

$$SAM(s_i, s_j) = \cos^{-1}\left(\frac{\sum_{l=1}^{L} s_{il}s_{jl}}{\left[\sum_{l=1}^{L} s_{il}^2\right]^{\frac{1}{2}}\left[\sum_{l=1}^{L} s_{jl}^2\right]^{\frac{1}{2}}}\right) \quad (2)$$

where $l = (1 \ldots L)$ is the number of spectral bands and s_i and s_j are the two spectra to be compared. The angle between the two spectra is proportional to their similarity. As reference spectra, we used the spectra of the reference windows shown in Fig. 1(a). SAM is a faster algorithm than SSR, as SSR involves the computation of the eigenvalues $M \times N + N$ times, where M is the number of pixels, N is the number of the reference windows, and the last N refers to the computation of the eigenvalues of the reference windows, which is time consuming. However, SAM does not take into consideration the neighborhood of the pixel. In addition to buildings, SAM enhances also other objects [Fig. 1(c)], which would further affect the recognition accuracy for buildings.

To discriminate between buildings and other enhanced structures in the SSR images, we applied the grayscale HMT.

III. Building Detection

A. Computing the HMT

The grayscale HMT uses the two fundamental operators of MM, which are erosion and dilation. In MM, the image is processed with a predefined pattern called structuring element (SE), which is used as a "probe" to examine a given image for specific properties. The origin of the SE defines the positioning of the SE at a given pixel. Erosion ε of f by SE B is defined as [12]

$$\varepsilon_B^f(x, y) = \wedge\left\{f_{(-b)}; b \in B\right\} \quad (3)$$

where $f(x, y)$ represents the value of a pixel in the image f with coordinates x and y, $\wedge$ is the infimum operator, and $f_{(-b)}$ is the translation of f by the vectors $-b$ of B [13]. Dilation δ of f by B is defined as [12]

$$\delta_B^f(x, y) = \vee\left\{f_{(-b)}; b \in B\right\} \quad (4)$$

where $\vee$ is the supremum operator.

The grayscale HMT is defined as (5) [13], shown at the bottom of the next page, where B_{FG} and B_{BG} are the SEs for the foreground and background, respectively.

The interval (the difference between erosion and dilation) is controlled by the parameters of the foreground and background SEs. However, a high interval would detect structures other

than buildings, while a low interval would miss buildings [14]. Instead, we examined the degree to which pixels in the image fit the SEs. To do this, we replaced the standard erosion and dilation by fuzzy erosion and dilation. Fuzzy erosion is represented by [15]

$$\varepsilon_B^{\mu_f}(x,y) = \wedge \min\left[1, \mu_f(x,y) + 1 - \mu(b)\right]. \tag{6}$$

Fuzzy dilation becomes

$$\delta_B^{\mu_f}(x,y) = \vee \max\left[0, \mu_f(x,y) + \mu(b) - 1\right] \tag{7}$$

where $b \in B$, $\mu(b)$ is the degree of membership to the SE B, and $\mu_f(x,y)$ is the degree of membership to the image. To set the values of the SSR images to the interval [0, 1], we used the S-shaped membership function [16]

$$\mu_f(x,y) = S\left(f(x,y,\alpha,\beta,\gamma)\right) \tag{8}$$

where the parameters α, β, and γ are expressed as

$$= \begin{cases} 0, & \text{if } lMin \le f(x,y) \le \alpha \\ 2\left(\frac{(f(x,y)-\alpha)}{(\gamma-\alpha)}\right)^2, & \text{if } \alpha < f(x,y) \le \beta \\ 1 - 2\left(\frac{(f(x,y)-\gamma)}{(\gamma-\alpha)}\right)^2, & \text{if } \beta < f(x,y) \le \gamma \\ 1, & \text{if } \gamma < f(x,y) \le lMax \end{cases}$$

$$\alpha = lMin + 0.05(lMax - lMin)$$

$$\gamma = lMax - 0.05(lMax - lMin)$$

$$\beta = \alpha + (\gamma - \alpha)/2$$

where $lMin$ and $lMax$ are the minimum and maximum for the gray values of the image.

B. Discriminating Between Buildings and "No Buildings"

To discriminate between buildings and "no buildings," we computed several HMTs, and we decreased the interval between the foreground and background SEs. Because higher SSR values corresponded to a higher potential to belong to buildings and the SSR values were transformed to the interval [0, 1] by the fuzzification in (8), we examined the fit to constant degrees of membership to the SEs for all SSR images. A high initial degree of membership (0.8) was set for the foreground SE, and a low initial degree of membership (0.1) was set for the background SE. In the consecutive iterations (computations of HMT), we decreased the degree of membership for the foreground SE and increased the degree of membership for the background SE (both by increments of 0.1). The aim of this was to examine the different response patterns to a decreasing interval when both SEs were placed over the object (i.e., over a building roof, over a bright object, or over the background). In Fig. 2, we show the typical responses to the decreasing interval. A turning point in the response pattern occurs when a complete fit to both SEs is achieved. After this, the HMT value begins to decrease because the eroded value remains one in the consecutive iterations, while the dilated value increases. Pixels on flat roofs will completely fit both SEs from the first iterations because they have high SSR values and are surrounded by pixels with high SSR values. As pixels on nonflat roofs may receive lower SSR values further from where their sections were connected, they may receive either an increasing or a constant HMT value in the first iterations. Pixels on bright structures may also achieve a complete fit to both SEs; however, this will occur in later iterations compared to pixels on flat and nonflat roofs. The HMT value for pixels located on the background only increases, because a complete fit to both SEs did not occur at all. Thus, according to when, at which iteration, the decrease of the HMT value began, we were able to discriminate between buildings and other bright structures. If we had used the standard erosion and dilation operators, we would not have obtained different response patterns, but only the number of pixels evaluated as positive would have changed.

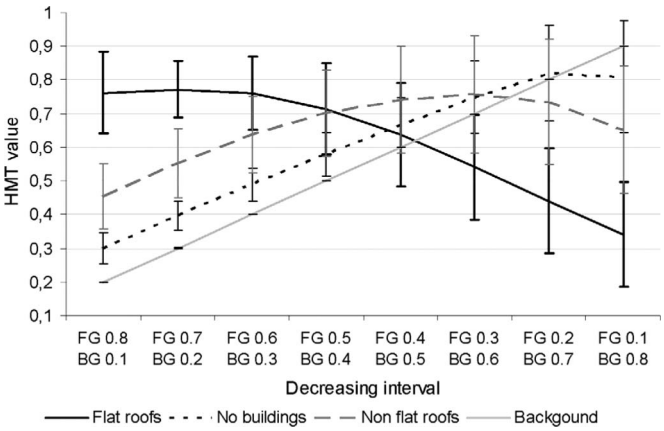

Fig. 2. Response of pixels to a decreasing interval. On the X-axis, the degree of membership to the SEs [(FG) foreground and (BG) background] is given. On the Y-axis, we show the value of the HMT. A sample of 20 pixels from subset 1 of the Ikonos image with brown-colored roofs was used for each situation (i.e., flat roofs, nonflat roofs, etc.) The mean and a one standard deviation from the mean are plotted.

The slope of the curve (Fig. 2), as opposed to examining a single interval, highlights the difference of buildings versus the background and "no buildings." Although the opening by reconstruction morphological profile [4] could be used to detect bright structures on a dark background, it would only detect buildings with flat roofs, because only pixels with a strong similarity to their surrounding region produce a high response in the output level of the profile [17]. The fuzzy HMT measures the ratio between the number of pixels that fit the configuration of SEs and the total number of pixels in the area covered by the SEs [5]. However, in the case of SSR images, it would return similar values for buildings and "no buildings."

$$\left[HMT_B(f)\right](x,y) = \begin{cases} \left[\varepsilon_{B_{\mathrm{FG}}}(f)\right](x,y) - \left[\delta_{B_{\mathrm{BG}}}(f)\right](x,y), & \text{if } \left[\varepsilon_{B_{\mathrm{FG}}}(f)\right](x,y) > \left[\delta_{B_{\mathrm{BG}}}(f)\right](x,y) \\ 0, & \text{otherwise} \end{cases} \tag{5}$$

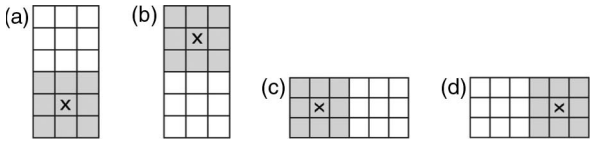

Fig. 3. Designed configurations for SEs. Foreground SE in gray and background SE in white; x is the origin of the SE.

C. Defining the Configurations of SE

For accurate recognition with the HMT, the size and shape of the SEs have to be defined correctly. To match the inner parts of the buildings, we used small square windows of 3 × 3 pixels for both SEs (Fig. 3). We used the configuration shown in Fig. 3(a) because changing the location of the background SE with regard to the foreground SE (i.e., bottom [Fig. 3(b)], right Fig. 3(c), or left [Fig. 3(d)]) did not change the number of detected objects but only their shape. As we are interested in locations and not in shape, these additional configurations were not used to save computational time.

D. Assigning Pixels to Buildings

To assign pixels to buildings, after each iteration, we compared the HMT value with that of the previous iteration. To retain only pixels that belong to building roofs, either flat or nonflat, pixels whose HMT value decreased or did not change were assigned to buildings. To automatically stop the iterations, we used the local homogeneity index [18]. Its computation includes the following steps:

$$S_{xy} = \sqrt{\frac{1}{n_W} \sum_{f(x,y)\in W_d(P_{xy})} (f(x,y) - m_{xy})^2} \qquad (9)$$

where S_{xy} is the standard deviation at pixel P_{xy}, $f(x,y)$ is the intensity of the pixel P_{xy}, m_{xy} is the mean of the n_W intensities within the window $W_d(P_{xy})$, which has a size of d by d and is centered at P_{xy}, and n_w is the number of pixels.

A measure of the discontinuity D_{xy} at pixel P_{xy} is

$$D_{xy} = \sqrt{G_x^2 + G_y^2} \qquad (10)$$

where G_x and G_y are the gradients at pixel P_{xy} in the x-direction (horizontal) and y-direction (vertical), respectively. To compute the gradient, we approximated the partial derivative in the horizontal direction with the central difference between columns and in the vertical direction with the central difference between rows, based on Prewitt kernel [19]. The standard deviation and the discontinuity are normalized by the maximum values of the standard deviation $(S_{\max})$ and the discontinuity $(D_{\max})$ of the image, respectively. Finally, the homogeneity H_{xy} at P_{xy} can be written as

$$H_{xy} = 1 - \left(\frac{S_{xy}}{S_{\max}}\right) \times \left(\frac{D_{xy}}{D_{\max}}\right). \qquad (11)$$

The index gives values from zero to one. Higher values correspond to higher homogeneity. An empirically defined threshold was set to 0.85 for Ikonos images and 0.75 for GeoEye images. To stop the iterations, after each iteration, we computed the mean value of the local homogeneity index for the retained pixels. When this mean exceeded the defined threshold, the iterations were stopped. Finally, all of the binary images were combined.

TABLE I
RESULTS OF BUILDING DETECTION

	Ikonos subsets					GeoEye subsets		
	1	2	3	4	5	1	2	3
Size (in pixels)	512x 512	400x 400	906x 216	400x 400	460x 480	219x 384	250x 350	340x 380
Number of buildings	164	182	97	140	115	142	288	329
Rate of recognition (%)	87%	78	84	90	85	85	82	74
Rate of correct identification (%)	95	90	62	91	88	85	92	77

IV. RESULTS AND DISCUSSION

We tested our method on eight image subsets taken from Ikonos and GeoEye images over residential areas in Sherbrooke, QC, Canada. The buildings had different orientations and sizes. The density of the buildings varied from low (subset 5, Ikonos) to high (subset 2, GeoEye).

To estimate the performance of our method, we computed the rate of recognition (the percent of correctly recognized buildings of all the buildings in the image subset) and the rate of correct identification (the percent of correctly recognized buildings of all the recognized locations). The results (Table I) show certain consistencies: Despite differences between the residential areas and sensors, almost the same relatively high rate of recognition, varying from 74% to 90%, was achieved for all of the subsets. Except for subset 3 of Ikonos, the method achieved a high percentage of correct recognition, ranging from 77% to 95%.

Some detection results are shown in Fig. 4. They demonstrate the method efficiency to detect buildings with different sizes and orientations. Partial occlusion, which usually causes omission errors when detecting buildings in VHSR images, did not affect the recognition accuracy of our method: Buildings that were partially occluded by trees were also detected [Fig. 4(c) and (d)]. Except for the definition of the reference windows, the method is automated. By close observation on the detection results, we found that buildings situated close together may be misinterpreted as one building, large buildings may be misinterpreted as several small ones, and large areas covered by bare soil were sometimes erroneously detected as buildings near their edges. Those could be improved by using an adaptive threshold on the local homogeneity index image, rather than a constant threshold value.

In some subsets, roads had the same color as some building roofs, white or light blue, and were also detected. However, in the results of the HMT, roads appeared disconnected from buildings. As the size of roads is larger than that of the buildings, we simply applied the size criteria to discriminate between roads and buildings. An example of the results before and after this additional processing is shown in Fig. 5. The roads were completely removed, while the number of detected buildings remained the same.

Compared to other building detection methods applied to the same Ikonos image, the extraction performance of our approach was among the best results. In [20], 86% accuracy for the

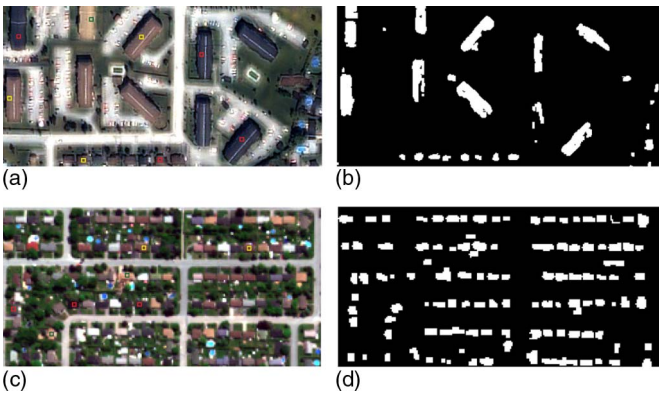

Fig. 4. Results for (top row) Ikonos and (bottom row) GeoEye. (a) and (c) True color composites. (b) and (d) Results. Examples of the locations of reference windows are shown in the true color composites as squares. Red squares correspond to a blue roof color, green squares to a beige roof color, and yellow squares to a brown roof color.

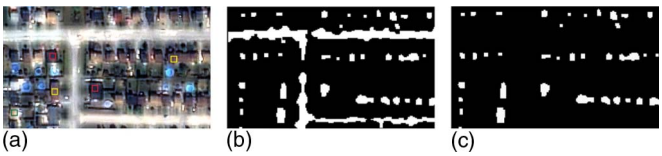

Fig. 5. Removing roads from an Ikonos image. (a) True color composite. (b) Results before road removal. (c) Results after road removal.

detection of new buildings was achieved based on multispectral image segmentation and object rule-based classification. The parameters for the segmentation were defined automatically but were derived from ancillary data. The method proposed in [2] uses the panchromatic band of Ikonos. To detect buildings, it estimates the difference in the variance of the gray values over the building and over its periphery. It achieves means of 82.5% for the rate of recognition of buildings and 74.8% for the rate of correct identification. With our method, we obtained means of 85% and 85.7%, respectively. The successful performance of our method was probably due to the initial enhancement of the building locations and the use of a specific algorithm to detect buildings, instead of detecting all objects in the image as was done in [20]. Furthermore, the use of spectral information, as compared to the method in [2], also contributed to the accuracy of our model.

V. Conclusion and Future Work

We have proposed a new method for building detection based on spectral and contextual information. Grayscale images were generated from multispectral images in order to enhance potential building locations based on the spectral similarity of roofs, taking into consideration the correlation between bands. The HMT was applied to these images in order to assign pixels to buildings. We tested our method on subsets of Ikonos and GeoEye images. The results were consistent despite differences in the characteristics of the residential areas that were analyzed. Our method compared favorably with two other methods applied to images of Sherbrooke, QC, Canada.

The method provided reliable building detection when using only spatial information would not have been sufficient. Future work will focus on decreasing the user intervention required to define classes and on decreasing the computational complexity of the SSR.

References

[1] E. Baltsavias, "Object extraction and revision by image analysis using existing geodata and knowledge: Current status and steps toward operational systems," *ISPRS J. Photogramm. Remote Sens.*, vol. 58, no. 3/4, pp. 129–151, Jan. 2004.

[2] S. Lhomme, D.-C. He, C. Weber, and D. Morin, "A new approach to building identification from very-high-spatial-resolution images," *Int. J. Remote Sens.*, vol. 30, no. 5, pp. 1341–1354, Mar. 2009.

[3] J. A. Benediktsson, M. Pesaresi, and K. Arnason, "Classification and feature extraction for remote sensing images from urban areas based on morphological transformations," *IEEE Trans. Geosci. Remote Sens.*, vol. 41, no. 9, pp. 1940–1949, Sep. 2003.

[4] X. Jin and C. H. Davis, "Automated building extraction from high-resolution satellite imagery in urban areas using structural, contextual, and spectral information," *EURASIP J. Appl. Signal Process.*, vol. 2005, pp. 2196–2206, Jan. 2005.

[5] S. Lefèvre, J. Weber, and D. Sheeren, "Automatic building extraction in VHR images using advanced morphological operators," in *Proc. IEEE/ISPRS Joint Workshop Remote Sens. URBAN*, Paris, France, 2007, pp. 1–5.

[6] B. Naegel, N. Passat, and C. Ronse, "Grey-level hit-or-miss transforms—Part I: Unified theory," *Pattern Recognit.*, vol. 40, no. 2, pp. 635–647, Feb. 2007.

[7] J. Weber and S. Lefèvre, "A multivariate hit-or-miss transform for conjoint spatial and spectral template matching," *Lecture Notes in Computer Science: Image and Signal Processing*, vol. 5099, pp. 226–235, Jul. 2008.

[8] B. Sırmacek and C. Unsalan, "Urban-area and building detection using SIFT keypoints and graph theory," *IEEE Trans. Geosci. Remote Sens.*, vol. 47, no. 4, pp. 1156–1167, Apr. 2009.

[9] S. Bae, L. Udpa, S. Udpa, and T. Taylor, "Classification of ultrasonic weld inspection data using principal component analysis," in *Review of Progress in Quantitative Nondestructive Evaluation*, D. O. Thompson and D. E. Chimenti, Eds. New York: Springer-Verlag, Jun. 1997, vol. 16, pp. 741–748.

[10] D.-C. He and L. Wang, "Color preserving fusion of multiresolution images," *J. Commun. Comput.*, vol. 7, no. 9, pp. 36–44, 2010.

[11] F. Kruse, A. Lefkoff, J. Boardman, K. Heidebrecht, A. Shapiro, P. Barloon, and A. Goetz, "The spectral image processing system (SIPS)-interactive visualization and analysis of imaging spectrometer data," *Remote Sens. Environ.*, vol. 44, no. 2/3, pp. 145–163, May/Jun. 1993.

[12] J. Serra, *Image Analysis and Mathematical Morphology*. London, U.K.: Academic, 1982, pp. 431–432.

[13] P. Soille, *Morphological Image Analysis: Principles and Applications,* 2nd ed. Berlin, Germany: Springer-Verlag, 2003, pp. 142–146.

[14] B. Perret, S. Lefèvre, and C. Collet, "A robust hit-or-miss transform for template matching applied to very noisy astronomical images," *Pattern Recognit.*, vol. 42, no. 11, pp. 2470–2480, Nov. 2009.

[15] D. Sinha and E. Dougherty, "Fuzzy mathematical morphology," *J. Vis. Commun. Image Represent.*, vol. 3, no. 3, pp. 286–302, Sep. 1992.

[16] S. Intajag, K. Paithoonwatanakij, and A. Cracknell, "Automatic image segmentation using fuzzy hit or miss and homogeneity index," *Int. J. Remote Sens.*, vol. 27, no. 1, pp. 203–221, Jan. 2006.

[17] M. Klaric, G. Scott, C.-R. Shyu, and C. Davis, "Automated object extraction through simplification of the differential morphological profile for high-resolution satellite imagery," in *Proc. IGARSS*, 2005, pp. 1265–1268.

[18] H. Wang and D. Suter, "Color image segmentation using global information and local homogeneity," in *Proc. VIIth Digit. Image Comput., Tech. Appl.*, C. Su, H. Talbot, S. DOurselin, and T. Adriaansen, Eds., Sydney, Australia, Dec. 10–12, 2003, pp. 89–98.

[19] D. V. Rao, S. Patil, N. A. Babu, and V. Muthukumar, "Implementation and evaluation of image processing algorithms on reconfigurable architecture using C-based hardware descriptive languages," *Int. J. Theor. Appl. Comput. Sci.*, vol. 1, no. 1, pp. 9–34, 2006.

[20] M. Bouziani, K. Goita, and D.-C. He, "Rule-based classification of a very high resolution image in an urban environment using multispectral segmentation guided by cartographic data," *IEEE Trans. Geosci. Remote Sens.*, vol. 48, no. 8, pp. 3198–3211, Aug. 2010.